A UV DETECTOR FOR MICROFLUIDIC DEVICES

by

AMOS WELDEGEBRIEL

B.S., University of Asmara, 2008

A THESIS

Submitted in partial fulfillment of the requirements for the degree

MASTER OF SCIENCE

Department of Chemistry
College of Arts and Sciences

KANSAS STATE UNIVERSITY
Manhattan, Kansas

2014

Approved by:

Major Professor
Christopher T. Culbertson

Copyright

Abstract

Chemical separation involves selective movement of a component out of a region shared by multiple components into a region where it is the major occupant. The history of the field of chemical separations as a concept can be dated back to ancient times when people started improving the quality of life by separation of good materials from bad ones. Since then the field of chemical separation has become one of the most continually evolving branches of chemical science and encompasses numerous different techniques and principles. An analytical chemist's quest for a better way of selective identification and quantification of a component by separating it from its mixture is the cause for these ever evolving techniques. As a result, today there are numerous varieties of analytical techniques for the separation of complex mixtures. High Performance Liquid Chromatography (HPLC), Gas Chromatography (GC), Capillary Electrophoresis (CE) and Gel Electrophoresis are a few out of a long list. Each these techniques manipulates the different physical and chemical properties of an analyte to achieve a useful separation and thus certain techniques will be suited for certain molecules. This work primarily focuses on the use of Capillary Electrophoresis as a separation technique. The mechanism of separation in Capillary Zone Electrophoresis and principles of UV detection will discussed in chapter one.

Chapter two contains a discussion about the application of Capillary Electrophoresis (CE) on microfluidc devices. This will include sections on: microfabrication techniques of PDMS and photosensitized PDMS (photoPDMS), a UV detector for microfluidic devices and its application for the detection of wheat proteins.

In Chapter three we report the experimental part of this project which includes; investigations on the effect of UV exposure time and thermal curing time on feature dimensions of photoPDMS microfluidic device, investigations on the injection and separation performances of the device, characterization of a UV detector set up and its application for the separation and detection of wheat gliadin proteins. The results of these investigations are presented in chapter four.

Table of Contents

List of Figures

List of Tables

Acknowledgements

I would like to take this opportunity to thank everyone who helped me in the completion of my graduate study.

Dr. Culbertson, thank you very much for all your help and support and for taking time to discuss this project with me.

The Culbertsons Group, I really enjoyed working with all of you. Thank you all for being there.

I would like to thank my committee members Dr. Daniel Higgins and Dr. Jun Li.

I would also like to thank chemistry department staff: Ron Jackson, Tobbe Eggers, Jim Hodgson and the administration personnel's.

Dedication

I would like to dedicate this work to my parents – my father Michael Weldegebriel and my mother Elsa Berhane.

Chapter One

Introduction

Chemical separation involves selective movement of a component out of a region shared by multiple components into a region where it is the major occupant. The history of the field of chemical separations as a concept can be dated back to ancient times when people started improving the quality of life by separation of good materials from bad ones. Since then the field of chemical separation has become one of the most continually evolving branches of chemical science and encompasses numerous different techniques and principles. An analytical chemist's quest for a better way of selective identification and quantification of a component by separating it from its mixture is the cause for these ever evolving techniques. As a result, today there are numerous varieties of analytical techniques for the separation of complex mixtures. High Performance Liquid Chromatography (HPLC), Gas Chromatography (GC), Capillary Electrophoresis (CE) and Gel Electrophoresis are a few out of a long list. Each these techniques manipulates the different physical and chemical properties of an analyte to achieve a useful separation and thus certain techniques will be suited for certain molecules. This work primarily focuses on the use of Capillary Electrophoresis as a separation technique.

Furthermore, I will discuss about the application of Capillary Electrophoresis (CE) on microfluidic devices. This will include sections on: microfabrication techniques of PDMS and photosensitized PDMS (photoPDMS), a UV detector for microfluidic devices and its application for the detection of wheat proteins.

1.1 Introduction to Capillary Electrophoresis (CE)

Capillary electrophoresis, as the name indicates, is electrophoresis performed in an open tube that is filled with a conductive buffer. The open tube, a capillary, has a very small inner diameter on the order of tens to few hundreds of microns (5-300μm), and is tens of centimeter long (25-75cm). The capillary material can be fused silica, a polymer like Teflon or a fluidic network on a microfluidic device where the channel length, width and depth vary accordingly. The small inner diameter of a capillary offers a high surface to volume ratio which allows the efficient dissipation of heat when an electric field is applied. Moreover the anticonvective nature of CE enhances the separation quality by reducing undesirable mixing due to turbulent flow. All these, plus other facts to be mentioned later result in a highly efficient separation. [1] The powerful potential of CE was first demonstrated by Jorgensen and Lukas in 1982 when they reported a buffer filled silica capillary column to separate charged particles. CE consists of relatively simple instrumentation, namely a fused silica capillary, a high voltage power supply, two buffer vials and a detector.

1.2 Modes of CE

Capillary Electrophoresis can be operated in a variety of modes, making it a handy tool for an analyst to approach an analytical problem in several ways. Accordingly capillary electrophoresis has versatile applications in various fields including, food analysis,[3, 4] pharmaceutical analysis, [5, 6] bioanalysis,[7] and environmental pollutants analysis.[8, 9] The main modes of CE are based on the separation mechanism and are as follows: (1) Capillary Zone Electrophoresis (CZE), a separation of analyte into zones based on their eletrophoretic mobilities in open capillaries with a relatively lower viscosity system.[10, 11] **(**2) Micellar Electrokinetic Chromatography, a separation of uncharged particles based on their partitioning between the micelles that serve as pseudo-

stationary phase and a separation buffer.[12,13] (3) Capillary Gel Electrophoresis, an electrophoretic separation based on molecular size in a gel/polymer filled capillary that serves as a molecular sieve.[14,15] (4) Capillary Isoelectronic Focusing, a separation based on manipulation of isoelectronic point differences of proteins to focus analytes in a capillary filled with a pH gradient using ampholites.[16] (5) Capillary Isotachophoresis, a separation of analytes based on their electrophoretic mobilities, however, in this mode the analytes are sandwiched consecutively between a fast moving and a trailing electrolyte as consequence of which the electropherograms does not return to the baseline.[17]

1.3 Electrophoretic mobility

Of the above mentioned modes Capillary zone electrophoresis (CZE) which separates analytes into zones of similar electrophoretic mobilities is the most commonly used CE mode due to its broad applicability to both the separation of cations and anions in a sample. In this mode, the ultimate separation of charged particles is achieved by electrophoretic mobilities of ions under the influence of electroosmotic flow.

A particle with a charge of q inside a capillary tube, under the influence of Electric field strength E (a function of applied voltage and capillary length in volts/cm), experiences an Electric force given by F_e

$$F_e = qE \qquad (1.1)$$

This electric force imparts a motion with a velocity (v) to the ion in proportion to the electrophoretic mobility of the ion μ_e which is the constant characteristic of the ion in a certain medium.

$$v = \mu_e E \qquad (1.2)$$

According to Stoke's Law the movement of an ion, with a velocity (v) and radius (r), in any medium of viscosity (η) imparted by the electric force is opposed by the inherent viscous forces of the solution, given by F_f

$$F_f = -6\pi\eta r v \qquad (1.3)$$

When the electric field is applied, the ion attains a steady state in 10^{-12} seconds were electric force and drag force are balanced, thus

$$qE = -6\pi\eta r v \qquad (1.4)$$

Rearranging equation 1.4 yields

$$v = \frac{qE}{6\pi\eta r} \quad \text{where} \quad \mu_e = \frac{q}{6\pi\eta r} \qquad (1.5)$$

This equation reveals the underlying principle of separation by Capillary Electrophoresis. As the right side of the equation indicates, mobility of the ions in a certain medium depends on their charge to hydrodaynamic ratio. Therefore a highly charged particle with a smaller size will move faster than a minimally charged particle with a larger radius. The differing electrophoretic mobilities of analytes in a solution will result in their separation accordingly.

1.4 Electroosmotic flow (EOF)

In addition to the electrophoretic velocity, a secondary phenomena known as electroosmosis occurs in small diameter capillaries. Electroosmotic Flow (EOF), a bulk fluid flow that originates from electroosmosis, can have a dramatic impact on particle's actual velocity.

The formation of an Electrical Double Layer (EDL) at the solid liquid interface of an insulator, such as the glass of a capillary, in contact with an electrolyte solution facilitates the bulk fluid movement of fluid when an electric field is applied across the length of the capillary. The motion of ions is referred to as the EOF. This fluid motion is a result of acid base equilibria with respect to silanol (SiOH) functional groups on the surface of the fused silica. Under buffer conditions of pH 2 and higher, these silanol groups dissociate to give a net negative charge on the surface of the fused silica. To maintain neutrality, these negatively charged surface ions attract some of the cations in the buffer solution and form a compact layer or Stern layer. The rest of ions in the buffer that is adjacent to the stern layer are mobile and form the diffuse layer. The potential difference at the boundary (also known as shear plane) between stern layer and diffuse layer surface is known as the zeta potential. [18] This potential decreases exponentially as the distance from the substrate surface increases until at a certain distance where the bulk solution is reached and electro neutrality is observed again. Figure 1.1 below depicts the origin of EOF

Once a voltage is applied, the hydrated cations in the diffuse portion of EDL move towards the cathode establishing the bulk fluid flow. The bulk fluid flow generated by EOF has a constant velocity denoted by v_{EOF}. Electroosmotic flow is relatively flat as compared to parabolic flow profile of pressure driven techniques such as HPLC. Figure 1.2 below illustrates the difference in flow profiles. This flat flow profile is one of the factors that contribute to the well marked

efficient separation of CE. The magnitude of EOF velocity in a capillary can be expressed by Smoluchowuski equation [19] as:

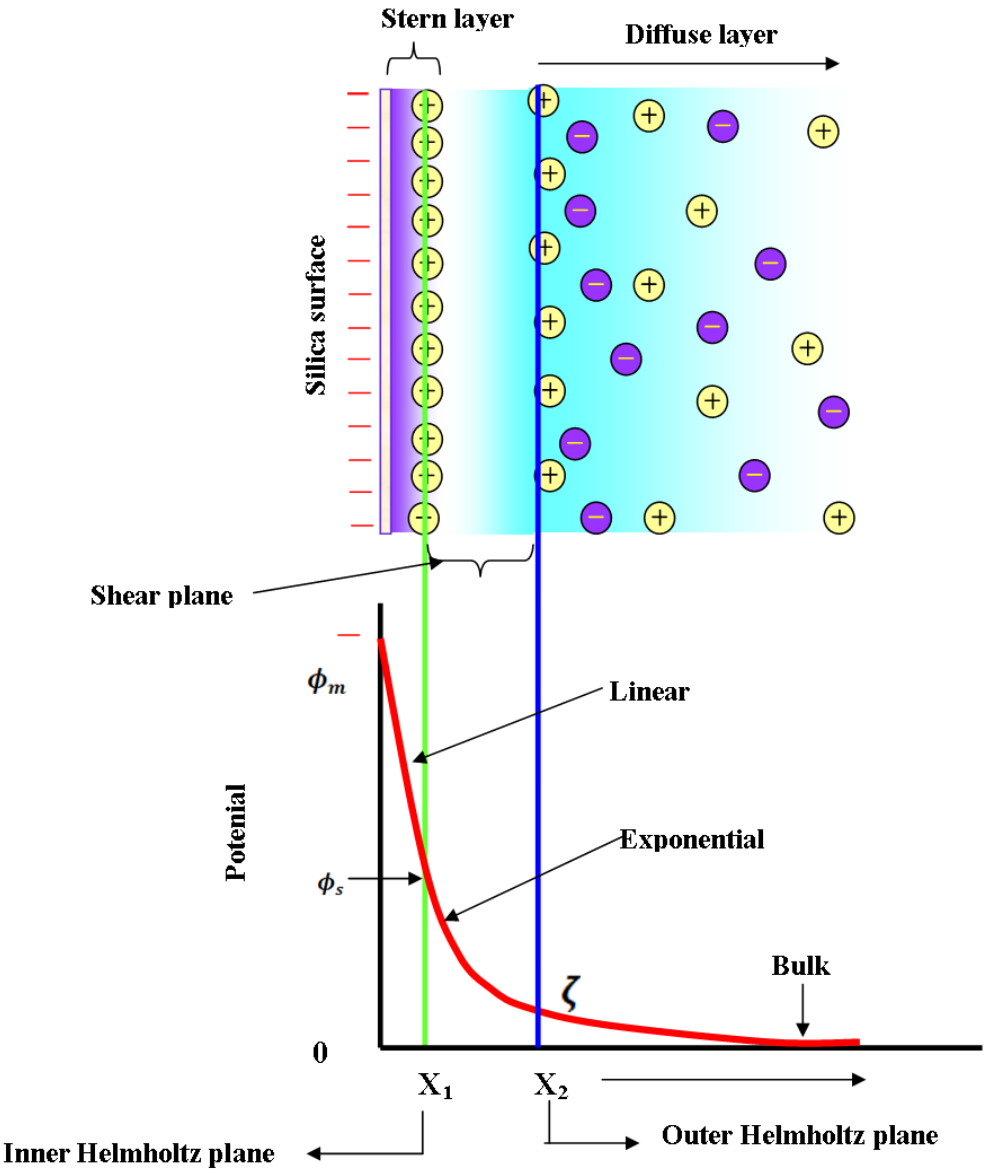

Figure 1.1. Electric Double Layer (EDL), ϕ is electric potential due to surface charge density. ζ is the zeta potential.

$$v_{EOF} = \left(\frac{\varepsilon\xi}{\eta}\right)E \quad \text{or} \quad v_{EOF} = \mu_{EOF}E \qquad (1.6)$$

Where ε is the permittivity of the medium, ξ is the Zeta potential and

$$\mu_{EOF} = \left(\frac{\varepsilon\xi}{\eta}\right) \qquad (1.7)$$

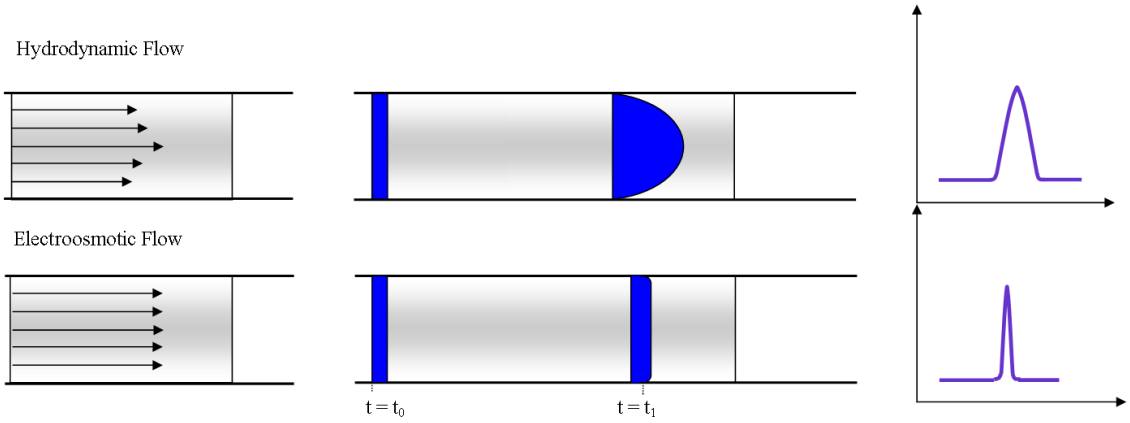

Figure 1.2. Velocity profile for pressure and electrokinetic driven flows in a capillary.

The total electrokinetic velocity (v_{ek}) of an analyte inside the capillary can be given by

$$v_{ek} = (\mu_{EOF} + \mu_{ep})E \qquad (1.8)$$

Electroosmotic mobility is often much greater in magnitude than the electrophoretic mobilities of the analytes. Figure 1.3 below illustrates the effect of electroosmotic flow on the actual velocity of a particle inside a capillary under the influence of applied electric field. Generally, small sized cations under the influence of EOF have the highest mobility towards the cathode owing to their largest charge to mass ratio . In contrast to these, small sized anions with a large negative charge tend to move towards the anode by electrophoresis, but since the EOF drag force towards the cathode is larger than their electrophoretic mobility towards the anode, the net movement is towards the cathode but at much slower velocity. Furthermore, neutral particles with a zero charge to mass ratio move at the velocity of the EOF towards the cathode. EOF plays a key role

by transporting all molecules (cations, anions and neutrals) towards the cathode end of the capillary. Consequently the detector will give signals at different migration times as the charged particles migrate toward the cathode.

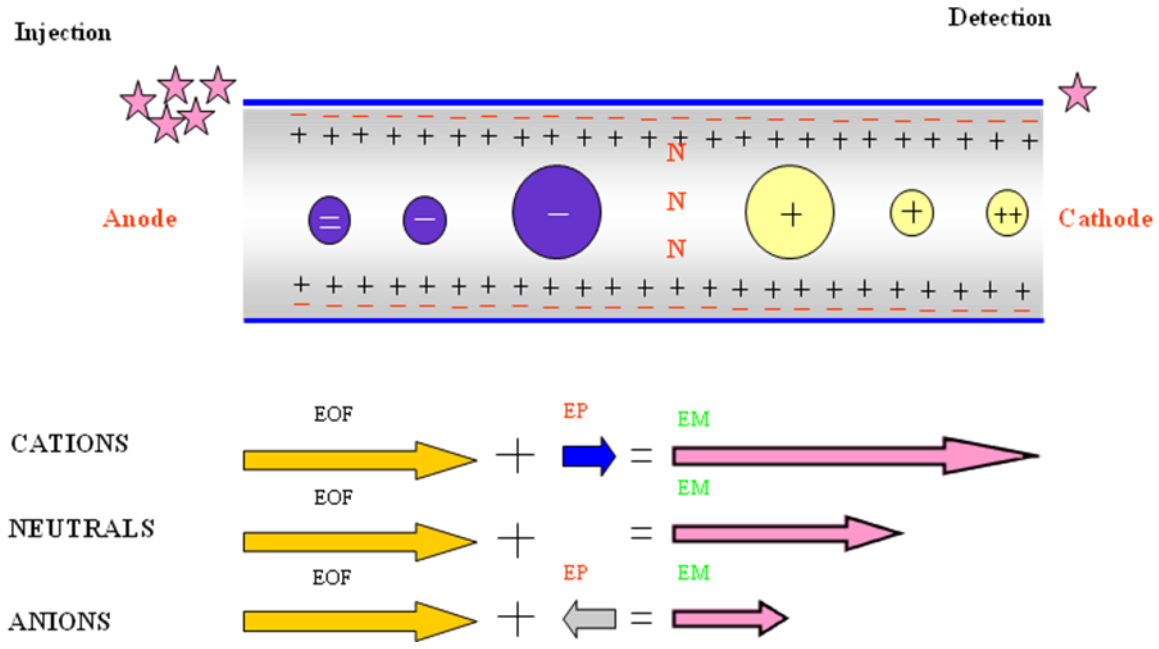

Figure 1.3. Differential migration of charged particles in a Capillary.

The surface charge on the capillary is strongly dependent on pH inside the capillary; as a result the zeta potential as well as EOF can be easily affected by changes in pH of the buffer used to fill the capillary. At higher pH (greater than two) the silanol group is deprotonated to form negatively charged silane groups leading to a greater EOF as compared to lower pH (less than two) were the silanol group will stay intact as a protonated group.

1.5 Instrumentation and operation

A schematic diagram of the relatively simple setup of CE is shown below. It consists of a capillary tube inserted into buffer vials on both ends. The capillary is usually about 25-100cm long and about 5-300µm internal diameter. The vial on the sample injection end of the capillary can be switched to the sample vial during injection. Hydrodynamic and electrokinetic injections are commonly used for injection of sample into the CE capillary. Hydrodynamic injection is

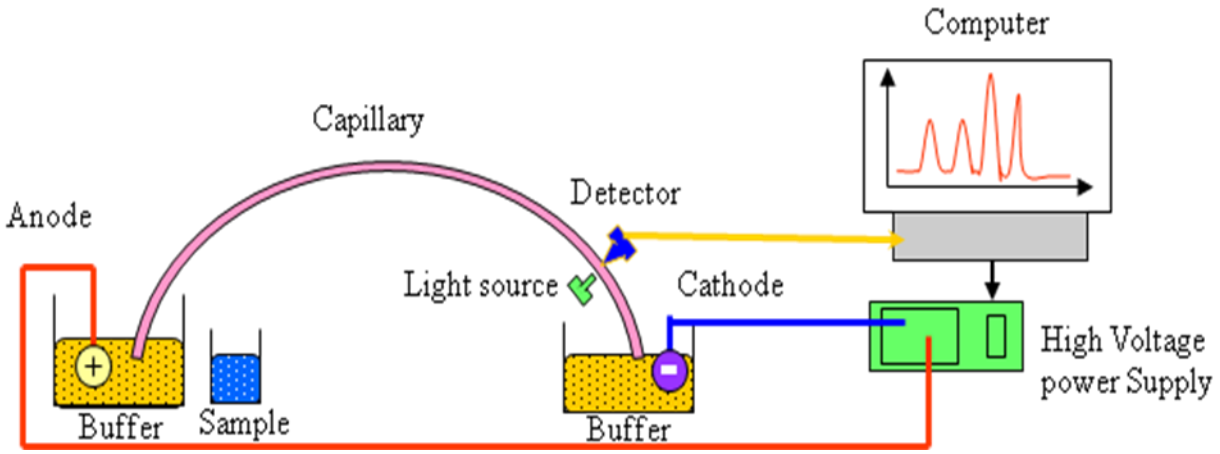

Figure 1.4. Capillary Electrophoresis set up.

based upon a pressure difference between the two ends of the capillary, while electrokinetic injections are based on the voltage difference across the two ends. The detector is normally placed closer to the other end of the capillary, the most commonly used detectors are UV-Vis and mass spectrophotometers. The two electrodes of the power supply (usually about 30kV) are inserted on the two buffer vials with the cathode usually on the detector end of the capillary. The buffer can be of different electrolyte strengths and pHs, and needs to be degassed and filtered before conducting the CE experiment. Surfactants and organic modifiers can also be loaded on the buffer vial.

1.6 Separation parameters

After the sample is injected and the high voltage is applied to the capillary, the analytes inside the capillary will migrate towards the cathode end of the capillary past the detector at different rates depending on their electrophoretic mobilities. The time it takes the analyte to migrate to the point of detection is called the migration time, denoted as (t_r). As the analyte passes the detection point, the intensity of the light source will decrease as compared to the blank and hence will be detected as signal for the detector. The plot of the different analyte migration times versus the signal recorded by the detector is referred to as the electropherogram. Such a plot is illustrated in the figure below. Two important separation efficiency indicators can be observed from the electropherogram. The width of a peak which is strongly influenced by dispersion processes and the distance between two peaks depends on the migration times of two different charged particles.

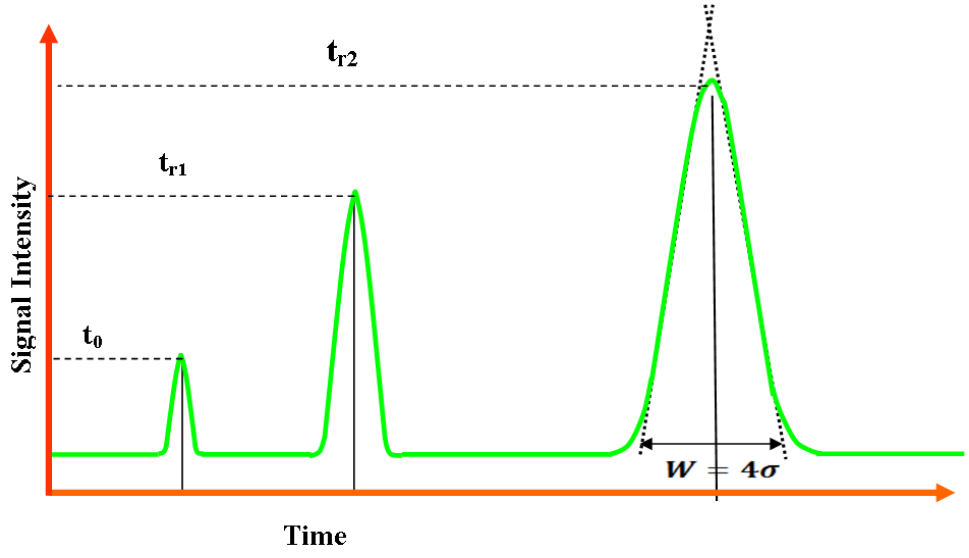

Figure1.5. Electropherogram.

1.6.1 Dispersion

As discussed earlier in section 1.2 CZE separates analytes into zones of similar electrophoretic mobilities. The different zones reach the detection point according to their respective migration times. The extent of each of these zones determines how long the intensity of light at the detection point will vary from the baseline. Therefore, the width of a peak in the electropherogram is proportional to the extent of a zone. The width of a zone is strongly affected by numerous factors that are collectively termed as sources of dispersion (band broadening). Although all the sources of dispersion contribute to the width of a peak, in order to develop a numerical description, it is necessary to set an assumption stating longitudinal diffusion to be the major contributor to zone length. Later in this section the numerical expression will be modified to account for all the sources of the dispersion.

Assuming an ideal condition, where all sources of dispersion except longitudinal diffusion are minimized, dispersion can be numerically described using Gaussian profile. The width of the peak at the base is given in terms of standard deviations (in time) of the Gaussian curve as

$$W_b = 4\sigma \qquad (1.10)$$

The variance σ^2 can be related to the diffusion coefficient D and migration time t as:

$$\sigma^2 = 2Dt \qquad (1.11)$$

Defining migration time t as l/v, where l is the distance to the detection point and v is the velocity of the particle, also described above as $\mu_e E$, the above equation can be rearranged to give

$$\sigma^2 = \frac{2Dl}{\mu_e E} \qquad (1.12)$$

The most important commonly used parameter describing the quality of the separation is the separation efficiency or the number of theoretical plates (N).

$$N = \frac{l^2}{\sigma^2} \qquad (1.13)$$

The number of theoretical plates generated by a separation can also be related to a parameter referred to as the height equivalent of theoretical plate (HETP or more commonly as H) by

$$H = \frac{l}{N} \qquad (1.14)$$

From equation (1.13) it becomes obvious the goal of efficient separation is to minimize the peak variance. At this point it is important to consider all the sources of band broadening including, longitudinal diffusion (σ^2_{diff}), injection plug length (σ^2_{inj}), joule heating (σ^2_{joule}), parabolic flow (σ^2_{flow}), detection system (σ^2_{det}), channel geometry (σ^2_{geo}), mass transfer (σ^2_{mt}), electrodisperssion (σ^2_{edisp}) and molecular adsorption (σ^2_{ads}). The equation below illustrates how these sources of band broadening can be summed to give the total dispersion.

$$\boldsymbol{\sigma^2_T = \sigma^2_{diff} + \sigma^2_{inj} + \sigma^2_{det} + \sigma^2_{edisp} + \sigma^2_{joule} + \sigma^2_{flow} + \sigma^2_{geo} + \sigma^2_{mt} + \sigma^2_{ads}} \qquad (1.15)$$

Substitution of equation 1.11 into equation 1.12 gives an equation that can relate the molecular diffusion of analyte to the separation efficiency in terms of number of theoretical plates.

$$N = \frac{\mu_e E l}{2D} = \frac{\mu_{ek} V}{2D} \qquad (1.16)$$

Equation 1.15 explains a very important feature of CE separation namely very efficient separation at high voltages. As it can be seen from the equation, application of high voltage significantly reduces the time the analyte spends in the capillary and hence less band broadening.

1.6.2 Resolution

The complete resolution of adjacent individual component peaks is the primary goal of any analytical separation. The resolution of two peaks in CE is given by

$$R = \frac{2(t_{r2}-t_{r1})}{w_1+w_2} = R = \frac{2(t_{r2}-t_{r1})}{4\sigma} \qquad (1.17)$$

Were, t_{r1} and t_{r2} are the migration times of the first and second peaks with peak widths w_1 and w_2 respectively.

1.7 CE Detection

Detection in CE is a challenge due to small sample injection, small peak volume and limited time to observe analytes. Despite these challenges a number detection techniques are available for CE absorbance, fluorescence, chemilumiscence and Refractive index detectors are few. A careful choice of these detectors may depend up on considering the response time and analytical figures of merit of these detectors. Out of the above mentioned detectors, absorbance detection is by far the most common due to: versatility, simplicity, ease of use, relatively cheap cost, compatibility with all CE modes, compatibility with most of buffers used and compatibility with the materials used to construct the capillary. More over absorbance detection is a non-destructive method. The largest limitation of absorbance detection is its relatively smaller detection limit.

1.7.1 UV-Vis absorbance Principle

UV-Vis refers to a region of the electromagnetic spectrum ranging from 190 to 800nm. In a CE system, when the analyte passes through the detector system, which is composed of a monochromatic light source aligned to a detector, the intensity (I_o) of the initial light source is reduced proportional to the concentration and molar absorptivity of the analyte. [20] At the

molecular level this reduction in intensity can be explained by excitation of valence shell electrons to higher orbital's. When sample molecules are exposed to UV-Vis light having an energy that matches a possible electronic transition within the molecule, some of the light energy will be absorbed as the electron is promoted from $n \rightarrow \pi^*$ or $\pi \rightarrow \pi^*$. This fact clearly indicates the need for a chromophore (an absorbing functional group) which in this case is π electrons or non-bonding valence shell electron pairs.

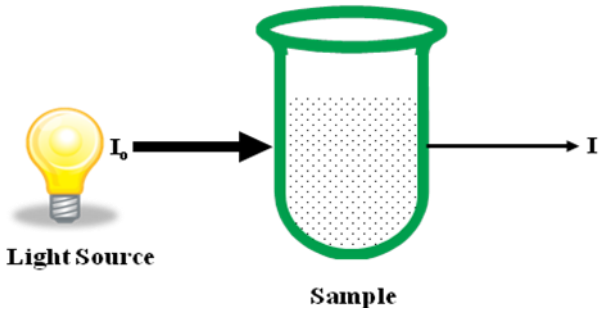

Figure1.6. Intensity loss due to absorbance.

The loss of intensity can be simply related to the concentration and molar absorptiviy of the molecule by Beer's Law, which is given by

$$A = \epsilon bC = -\log(T) = -\log\frac{I}{I_o} \qquad (1.18)$$

Where A is amount of light absorbed, ϵ is the molar absortivity of the analyte, b the distance the light travels in the sample holder, C is the concentration of the analyte and T is the transmittance (ratio of transmitted light to incident light).The sensitivity of CE UV-Vis absorption is mainly limited by the short path length of capillaries. A number of techniques including bubble cell, Z flow cell and sample pre concentration have been used to extend the path length of capillaries.

1.7.2 Instrumentation

The components of a UV-Vis detection system are illustrated in the figure 1.7 below. The main components are a light source, commonly a combination deuterium and tungsten lamps, a sample holder (cuvette), and a detector system which in this case is a Charge Coupled Detector (CCD) interfaced with a computer.

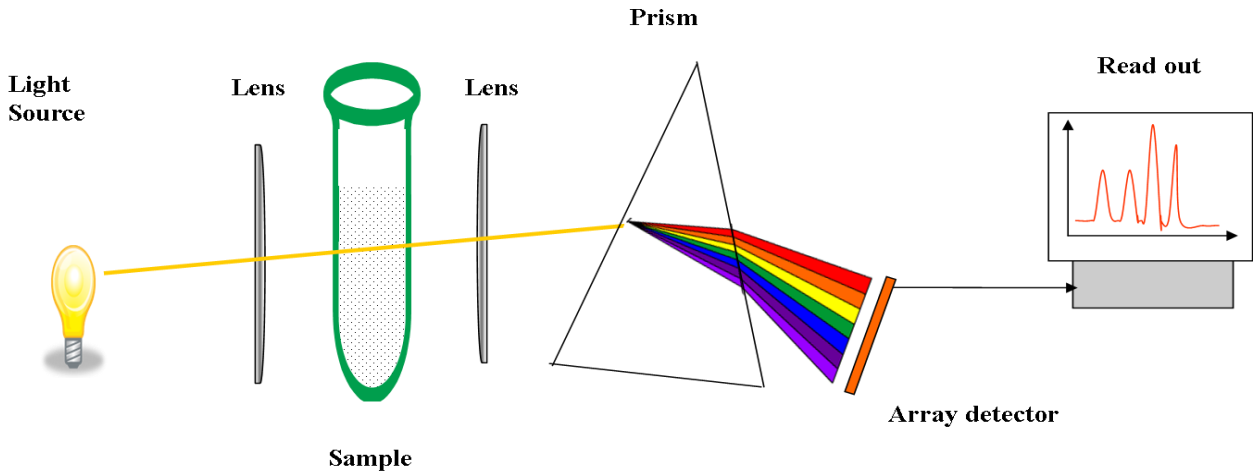

Figure 1.7. UV-Vis spectrophotometer set up.

Several types of light sources are available for UV-Vis absorbance including: the simple but incoherent atomic arc lamps such as deuterium arc lamp and tungsten halogen lamps and coherent laser light sources. Wavelength selection can be done either prior to passage though the capillary or after passage though capillary as illustrated in Figure 1.7. Wave length selection after passage though a capillary requires a diffraction grating and a multi-wavelength array detector. In CE, many of the most important analytical figures of merit such as sensitivity, detection limit and dynamic range can be strongly affected by the choice of the light source and the effective coupling of the light source into the capillary.[21]

1.7.3 Detection limit

Detection limit is defined as the lowest quantity of analyte that can be distinguished from the absence of the analyte (blank) at a stated statistical confidence limit. As discussed above the smallest amount of analyte that can be detected by absorbance detector is strongly affected by the path length of light which in CE is the inner diameter of the capillary. Although sample pre-concentration can be used, the easiest method of improving detection limit is to extend the path length. Rectangular capillary,[22] Z-cell,[23] and bubble cell[24] are some of the several methods for increasing the path length of the detection cell. Figure 1.8 below depicts these three approaches.

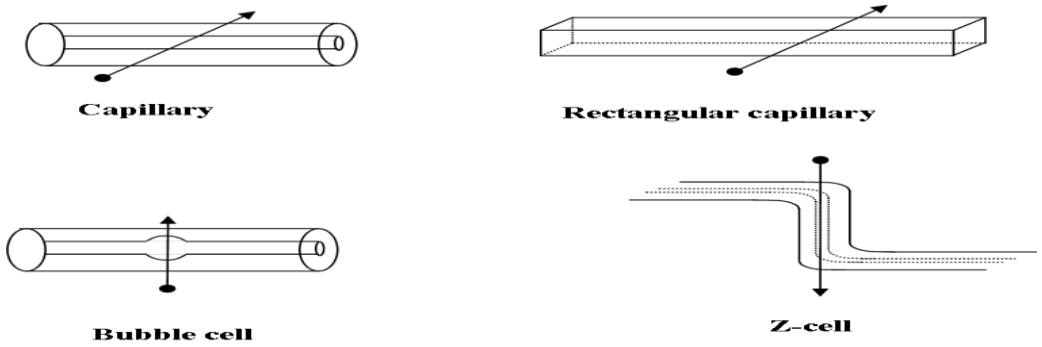

Figure 1.8. Methods of increasing path length of CE absorbance detector.

1.7.4 Linear Detection range

Stray light, defined as a unwanted amount of light that is usually of a different wavelength than the desired light, is one of the common problems that cause UV-Vis detectors to deviate from Beer's law. Higher analyte concentration is the second most common cause on deviation. Stray light causes the measured intensity to be erroneously high. Both these factors limit the linear detection range of the detector. The Effect of stay light can be adjusted by the equation 1.17

below. A slit or a pin hole can be used to reduce undesired light that is not coming directly from the sample cell, but that is at the cost of reducing the intensity of the light source.

$$A = \log \frac{I_0 + I_s}{I + I_s} \quad (1.19)$$

Summary

The first part of this chapter focused on presenting the principles that govern CE separations by explaining the origin of electrophoretic and electroosmotic mobility. Moreover separation parameters such as dispersion and resolution were discussed. In the second half absorbance method was discussed in detail. Chapter two will focus on the advantages of performing CE in a microfluidic device, fabrication techniques of microfluidic devices as well as designing of a suitable absorbance detector for microfluidic devices.

Chapter Two
Microchip Capillary Electrophoresis

2.1 Introduction

Current trends in modern analytical chemistry focus on miniaturization, simplification and automation of analytical methods. The goal of these trends is to realize easy to implement, self operating and small scale devices.[25] Microfluidics, which handles fluids in micrometer dimension channels, is one example of miniaturization in analytical chemistry. It offers a number of advantages over conventional analytical methods. The ability to use smaller quantities of reagents and samples to carry out separations with higher resolution and sensitivity and shorter analysis time are few of these advantages. Furthermore, these microchannels can be integrated in microchips and offer smaller footprints which allows multiplexing.[26] Microchip based separations such as Microchip Capillary Electrophoresis (MCE) is one of the many applications of microfluidics. The earliest application of MCE for separation dates back to 1992. [27] Since then, the field has grown exponentially in the number of investigators and areas of application. MCE quantitative analysis in the environmental, [28,29] biological, [30 ,31] and industrial field [32,33] are a few of the many applications.

Although conventional CE and MCE share the same mechanism of separation, there are many notable advantages of MCE over conventional CE. While conventional CE sometimes relies on pumps for hydrodynamic sample injection, MCE injections are done electrokinetically. This avoids the need for pumps. In MCE the separator channel does not need to be physically moved between buffer and sample reservoir, instead a crossing area between four connected reservoirs

is used as an injection method. The sizes of sample and buffer, as well as separation path length used in MCE are smaller as compared to conventional CE. The smaller sample injection plug further leads to decreased band broadening and increased separation efficiency.

The power supply for MCE, typically up to 5KV, is smaller as compared to 30KV for conventional CE. This can be explained by the 10 fold reduction in separation channel length in MCE as compared to conventional CE; consequently this leads to higher electric field. This higher electric field together with the reduced length of the separation channel is the basis for shorter separation time in MCE as compared to conventional CE. The reduction in separation time can further be explained from the equation below;

$$t = \frac{lL}{\mu_e V} \qquad 2.1$$

Where l is the effective separation channel length, L is the separation channel length, μ_e is the eletrophoretic mobility of the ion and E is the electric field. Reducing the separation path length and increasing the voltage results in shorter separation time. Furthermore, due to the small dimensions and high surface area to volume ratio of the channels, thermal transport is faster than in capillaries. This leads to better heat dissipation and smaller Joule heating problems. A variety of materials for fabrication of MCE including, fused silica, glass and polymers are available as compared to fused silica and Teflon for conventional CE. These materials offer easier and cheaper methods of fabrication as is discussed below.

2.2 Microchip Fabrication

2.2.1 Microchip fabrication materials

A variety of substrates are available for the fabrication of MCE devices. Generally they can be classified into silicon, glass/fused silica and polymers. Each of these substrates has its own advantages and disadvantages as will be discussed below briefly. A hybrid device which incorporates two or more of the above mentioned materials can also be fabricated. The choice of the ideal construction material might depend on various factors including, optical transparency, ease of fabrication, robustness, surface modification and others.

Silicon

The first microfluidic devices were based on traditional methods of fabricating microelectromechanical systems (MEMS) on silicon substrates due to the well-established fabrication methods available from the microelectronics industry.[34] But due to its non transparency, higher electrical conductance and biocompatibily concerns, silicon does not play much of a role to play in MCE, typically when optical method such as fluorescence or UV-Vis is the choice of detection.

Glass/Quartz

As compared to silicon, both glass and quartz are optically transparent. Glass has been used extensively in both conventional CE and MCE. [35] Some typical advantages of glass for on-chip CE include good dielectric properties, which allow it to withstand the high voltages used in electrokinetically driven flows and separations; good chemical resistance; amenability to surface modifications; as well as thermal and mechanical stabilities. However, glass has a UV cut off value of 300nm. Quartz on the other hand has superior optical transparency ranging from deep

UV to near IR regions of the electromagnetic spectrum. Even though quartz is the most commonly used material for conventional CE capillaries, it is the least used material for MCE due to several reasons. Relatively higher cost, slow etching rate due to its chemical inertness are a few. Moreover, both glass and quartz have other fabrication limitations including high cost of fabrication, involvement of dangerous chemicals (e.g., HF), difficulty of sealing process (high temperature, high pressure and super clean environment are normally required), difficulty of cell culturing and brittleness. [36]

Polymers

More recently, polymer based microchips have gained popularity over classic inorganic substrates such as glass due to their several inherent advantages. Fabrication requires relatively simple infrastructure and technologies (eliminating the need for sophisticated clean room facilities and equipment) and is commonly based on the use of replication-based microtechnologies. Moreover polymeric systems are less expensive than silicon and glass. [37] Several polymers, including poly(dimethylsiloxane) (PDMS), poly(methyl meth-acrylate) (PMMA), polycarbonate (PC), polyethylene terephthalate (PET), and polyester have all been used for their applications in various microchip capillary electrophoresis studies. [38]

2.2.1.1 PDMS

Among the above mentioned polymers PDMS is commonly used for several reasons: high fidelity replication of micron sized features, optical transparency down to 230nm, ability to cure at low temperature, chemical compatibility, strong elastic properties for portability, applicability for non-planar surfaces and the ability to reversibly seal with other PDMS surfaces and non

PDMS materials (10). Many of the appealing features of PDMS originate from its ability to form a silicone rubber with excellent elastic properties after being cross-linked. As can be seen from figure 2.1 PDMS features a repeating siloxane (Si-O) backbone with methyl groups on the silicon atoms.

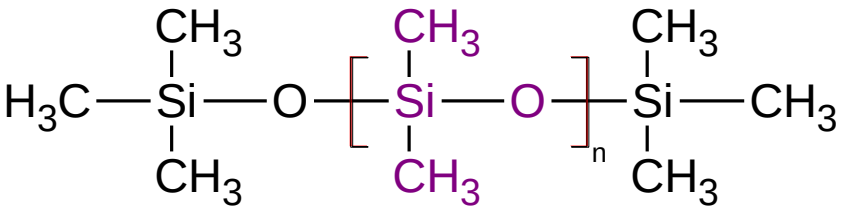

Figure 2.1. Structure of PDMS.

The siloxane bonds provide the polymer with a great deal of flexibility because they are able to rotate freely around the center of the bond. Commercial PDMS kit "Sylgard® 184" has three components which are important for the formation of the PDMS elastomer: the base which is composed of dimethlyvinyl terminated dimethyl siloxane precursor (figure 2.2 A), a curing agent which is mainly composed of dimethyl methylydrogen siloxane precursor (figure 2.2 B) and a platinium catalyst. A platinium catalyzed hydrosilylation reaction cross-links the two precursors to form a PDMS elastomer. When mixed, the hydride and vinyl groups react to form a 2-carbon linkage between silicon atom and different precursor molecules (figure 2.2 C). [39] The amount of cross linking depends on the quantity of the hydride containing precursor present in the mixture. If there is a sufficient degree of cross-linking between the precursors, the PDMS elastomer becomes a solid. The common proportion of base to curing agent is 10:1(w/w). The rate of the cross linking process can be increased by curing PDMS in an oven.

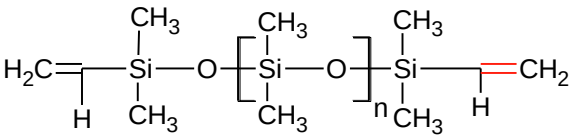

a, reactive vinyl groups

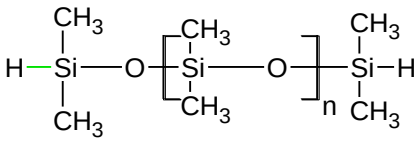

b, reactive hydride groups

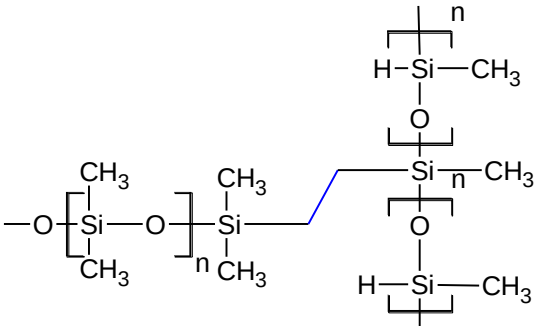

c, cross-linkage

Figure 2.2. (a) Reactive vinyl group, (b) reactive hydride group, (c) cross-linked PDMS elastomer.

Although PDMS has attractive features, it also suffers from a number of drawbacks including swelling upon contact with organic solvents, adsorption of small hydrophobic molecules on its surface, evaporation of water from channels and poorly defined unstable EOF. [40] Furthermore, PDMS elastomer cannot be photopatterned directly using photolithographic methods due to its chemistry, and hence a need for master template.[41] A number of investigations have been reported[42,43] to address these limitations. One such successful endeavor is making a photoPDMS.

2.2.1.2 Photo PDMS

An elegant way of directly fabricating PDMS is to make it photosensitive by incorporating photoinitiators in to the elastomeric network of PDMS and use it as a photoresist. Photo PDMS

offers a number of advantages over PDMS. The most obvious one is ability to directly fabricate using photolithography, this avoids the need for making a master template. Other advantages include relatively cheaper and shorter processing time per chip. To date, there have been several attempts to make photoPDMS by supplementing various photoinitiators to the commercially available Sylgard® 184.[44] One such successful attempt is addition of benzophenone, a white crystalline powder to initiate a free radical polymerization of PDMS using UV light. The proposed chemistry of photoPDMS is illustrated in figure 2.3 below

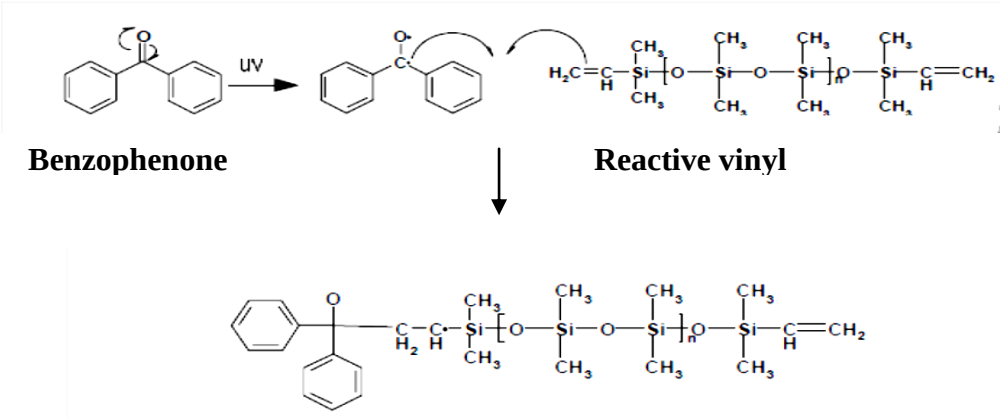

Figure 2.3. PhotoPDMS chemistry.

When a solution of benzophenone (benzophenone desolved in a suitbable solvent) is mixed with PDMS elastomer and irradiated using UV light < 365nm, a benzophenone radical is formed. Such reactive radicals react with the silicon hydride groups present in hydride containing precursor and the vinyl groups of the vinyl containing precursor. As a result benzophenone radicals prevent PDMS from undergoing traditional cross-linking. After post exposure baking, the unexposed PDMS gets cross linked while the unexposed regions remain uncross-linked and

can be washed away using a suitable solvent. A detailed procedure of of fabricating PDMS and photoPDMS are described below.

2.2.2 Microchip fabrication methods for PDMS

PDMS based microchip devices are fabricated via soft lithographic molding using a master template. Fabrication of master template using photolithography, which was first demonstrated by Duffy et al.[45] has gained popularity as a quick and cheap method. Photolithographic MCE device fabrication is discussed below in section 2.2.2.1

2.2.2.1 Photolithography

Photolithography is a technique that uses the irradiation of a photoactive resist to reproduce master template features from an original pattern, which is refered to as the "Photomask," on the surface of a substrate. Photoresists are organic polymers that undergo chemical reactions when exposed to light. This exposure to light changes the chemical and physical properties of the photoresist in a way such that its solubility in certain solvents before and after exposure to light will change noticeably. There are two classes of photoresists: negative tone and positive tone. Upon exposure to light, a positive tone photoresist undergoes reactions that weaken the polymerization network. A negative tone photoresits on the other hand undergoes reactions that strengthen the polymerization network. One such commonly used negative tone photoresist is SU-8. When exposed to Ultraviolet (UV) light SU-8 undergoes polymerization reaction that yields a high degree of cross linking which produces a very stable feature. In addition to this, SU-8 has many interesting features such as: ability to adhere to many substrates, uniformity upon spinning and relatively cheap cost.

Figure 2.4 below depicts a procedure for SU-8 master mold fabrication. SU-8 is spin coated to a desired thickness on a silicon wafer which is cleaned thoroughly using a cleaning protocol for silicon wafers. After spin coating, the SU-8 resist is subjected to "soft baking", where it is heated in order to remove most of the solvent in the resist and promote adhesion to the substrate.

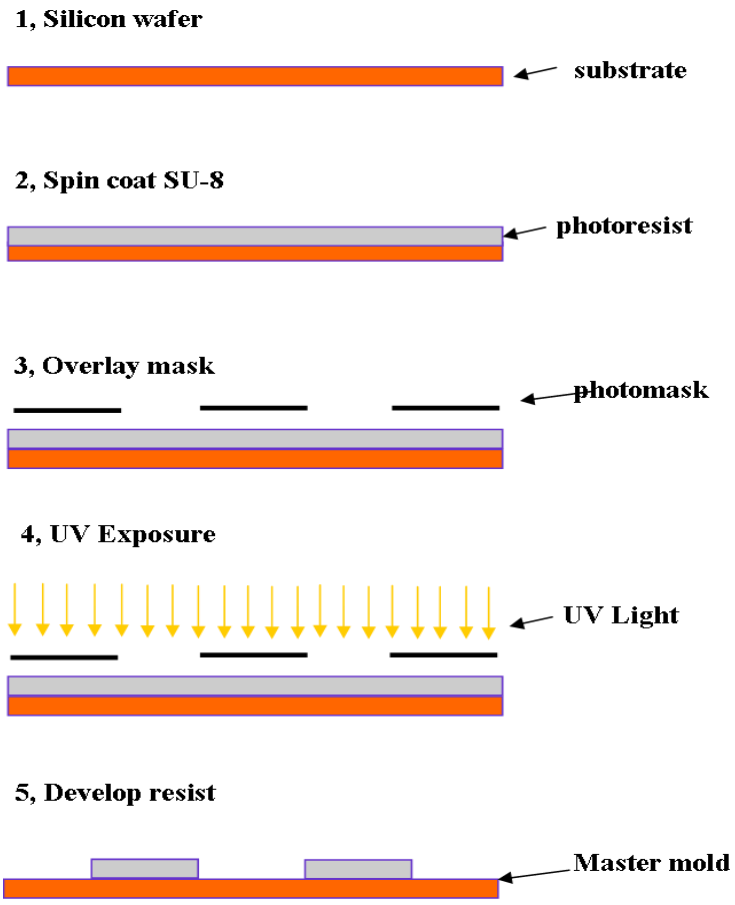

Figure 2.4. Master Mold fabrication steps.

After soft baking, a "photomask"; a transparency mask that contains transparent and opaque regions which make up the desired pattern, is placed in a direct contact with the surface of substrate. The transparent regions of the photomask are those that define the SU-8 area that need to be highly cross linked. The SU-8 coated substrate is then irradiated with a certain dose of light

intensity using a UV flood exposure system. After exposure the SU-8 coated substrate is heated once more. This heating step is called a "post exposure bake" and it helps to speed up the rate of the polymerization process. Finally after the silicon wafer is cooled down, it is developed by submersion in a solvent bath. The developer selectively removes the unexposed areas of the photoresit and the exposed regions are left behind as relief structures. The relief structure is the master template that defines the width and depth of the microchannel in the final PDMS device. At this point the mold for replicating the fluidic networks into above mentioned soft materials such as PDMS is ready. The next step is to copy these raised fluidic networks into PDMS. This can be done using Soft Lithography.

2.2.2.2 Soft Lithography

Soft lithography refers to a group of techniques which are used for replicating structures such as the relief structures of the master template in to a soft material such as PDMS. These techniques include microocontact printing, micromolding, and hot embossing. Soft lithographic methods offer a number of advantages over other microfabrication techniques including: ability to replicate 3D structures very quickly, cost effectiveness, ability to replicate hundreds of replica from a single master template, and high fidelity replication. Out of these three techniques, micromolding is the preferred method for replicating fluidic net works in a PDMS elastormer.

The chemistry of preparation of PDMS elastomer is described above in section 2.2.1.3 A. The PDMS elastomer is prepared by thorough mixing of the two PDMS precursors in a 10:1 (w/w) ratio of base and curing agent of the commercial kit. The PDMS elastomer is then degassed in a vacuum chamber and poured over the silicon wafer that contains the master template. After pouring, the PDMS elastomer is cured in an oven to speed up the cross-linking process. Once

cured, the solid but flexible PDMS chip can be peeled off the silicon wafer. Holes that provide fluid access to the microchannel network are punched on the chip and it is bonded to a flat substrate that can completely seal the fluidic network. Figure 2.5 below illustrates all the above mentioned steps. The device is now ready to be primed with surface modifiers and can be used for conducting CE experiments. This step finalizes the relatively cheaper but very long list of procedures for constructing a microfluidic device using PDMS. Making the master mold is a tedious process with many parameters that require careful attention and can prove to be time consuming if proper measures are not taken. An alternative to these is to make a photoPDMS that can be processed directly without the need to prepare a master template.

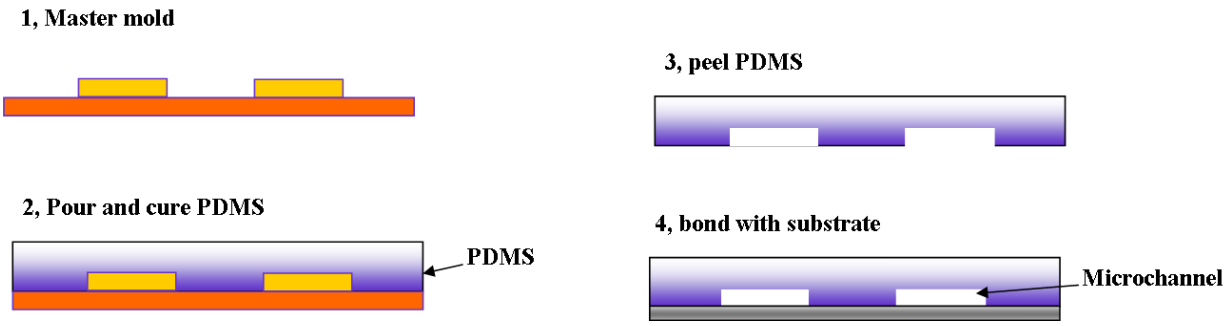

Figure 2.5. Micromolding of a PDMS device.

2.2.2.3 Microchip fabrication method for photoPDMS

The addition of benzophenone photoinitiator to commercial Sylgard® 184 renders it to behave as a positive tone resist as discussed in section 2.2.1.3 B. Therefore, photoPDMS can be processed using photolithography. The figure 2.6 illustrates the procedures involved in photoPDMS microchip fabrication. PhotoPDMS is spin coated to a desired thickness on a substrate of choice which is cleaned thoroughly using a cleaning protocol for silicon wafers. In this case, the

substrate will provide a support for the photoPDMS and can be selected depending on the desired application of the device. After spin coating, a photomask is aligned over the substrate and irradiated with a certain dose of light using a UV flood exposure system. Next, the photoPDMS is cured in an oven. This heating step helps to speed up the rate of the cross-linking of the unexposed regions, while the exposed regions stay uncured. Finally the substrate is cooled and developed by submersion in a solvent bath. The developer selectively removes the exposed areas of the photoresist and the exposed regions are left behind to define the microchip fluidic networks. A second quartz substrate that contains access holes for delivery of fluids into the fluidic networks is then used to seal the device.

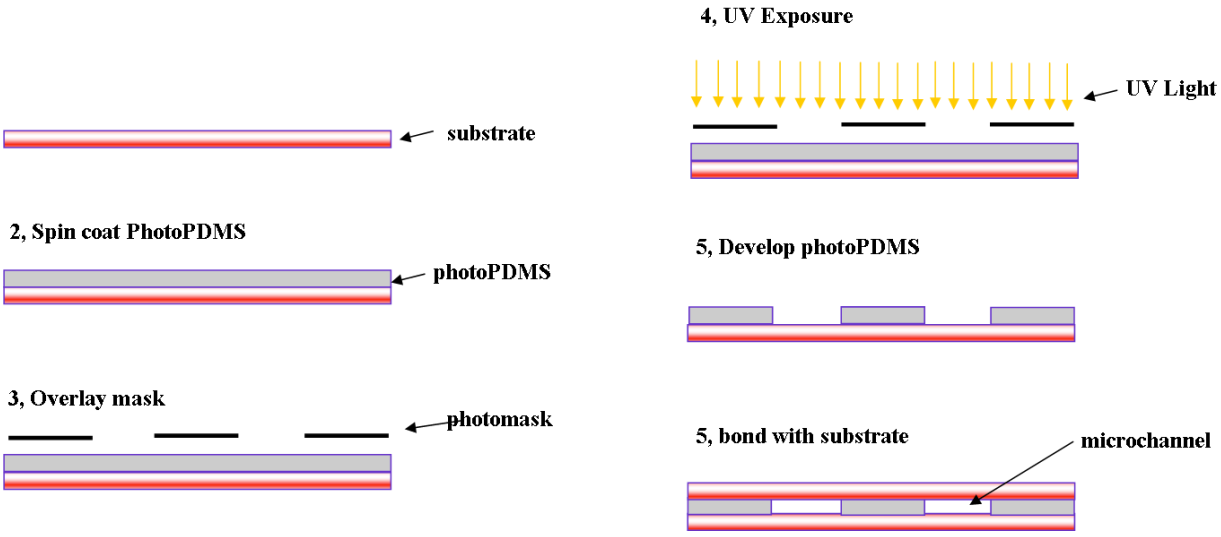

Figure 2.6. Fabrication of a hybrid substrate/photoPDMS/substrate device.

Finally the fluidic networks of this substrate/photoPDMS/substrate hybrid device can be primed with surface modifiers and is ready for conducting experiments. The general standard procedures for conducting experiments on a MCE device involve injection, separation and detection. These three steps are discussed below.

2.3 Injection

Sample injection in conventional CE is achieved by placing one end of the capillary tube into a sample vial either by applying pressure or voltage for a short period of time. This introduces a finite volume of sample into the capillary. Such a simple procedure cannot be applied for MCE injections, instead a new method of injection had to be devised. One such method is called gated injection. A gated injection contains a cross junction which an intersection point of two microfluidic channels, one that connects the sample access reservoir to the detection area and another that connects the buffer access reservoir to the waste collection reservoir. This is illustrated in figure 2.7 below. The fluidic network right below the intersection area is called the separation channel while the other one next to it called the waste channel.

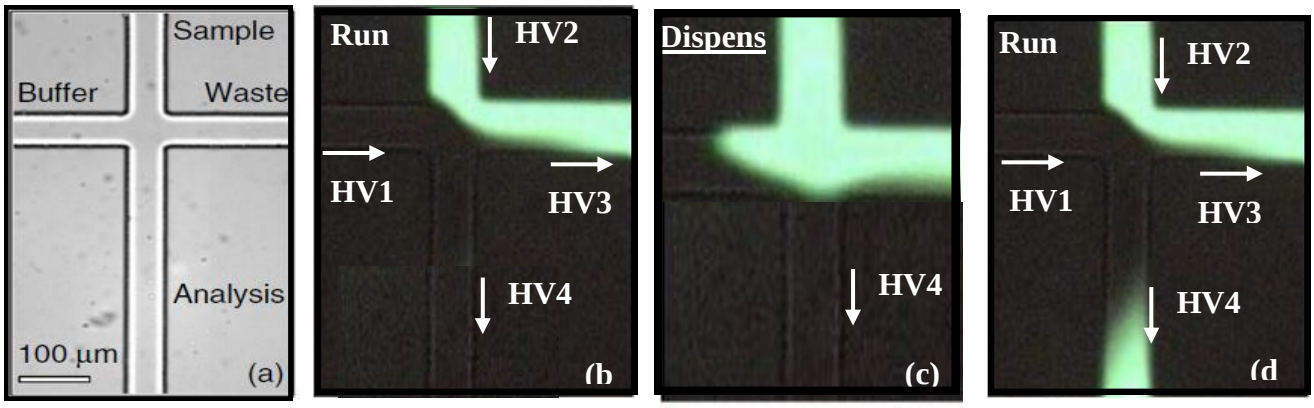

Figure 2.7. Electrokinetic injection in MCE device.

Using electrokinetic transport, a sample and separation buffer can be brought in contact at the intersection, upon fast switching of the voltages a small sample plug can be injected into the separation channel where the anlytes are separated and detected. An injection is depicted in

figure 2.7d. The voltage at the intersection of multiple channels can be calculated using a combination of Ohm's Law (2.2) and Kirchhoff's Rule (2.3).

$$V = IR \qquad (2.2)$$

$$\sum_{k=1}^{n} I^k = 0 \qquad (2.3)$$

Kirchhoff's current Rule state that the current into an intersection is equal to the current out of the intersection. Using this anlong with measured channel resistances, the voltage at the intecsection can be calculated. The electric field of the separation channel can be calculated using the voltage drop from the channel intersection to end of the sparation channel and the length of the separation channel using E= V/L. Therefore, two operational modes can be defined: the "Run mode/Analysis mode" in which the electric field of the separation channel is greater than the electric field of the waste channel, and the "Injection mode" which is the exact opposite of the run mode. This way switching the injection mode for a certain period of time introduces a defined sample plug in to the separation channel.

2.4 Separation

Separation of the injected sample plug occurs in much the same way as in conventional CE. The details of separation in narrow bore such as a capillary or a microfluidic network have been discussed in section 1.3 and 1.4 of chapter one. The injection time is generally marked as the zero time of separation. After injection analytes of the sample will start migrating toward the detector according to their actual velocities which are imparted by both the electrophoretic mobility and EOF.

2.5 Detection

Detection of analyte on a MCE requires a sensitive detection method due to the small detection cell and the small sample plug used. A number of such methods are available including laser induced fluorescence (LIF), mass spectrometry, electrochemical detection and absorption detection. LIF detection is the most common method due to its high sensitivity. But like any other method it has several limitations. One such notable disadvantage is the need for derivatization because most analytes are not fluorescent at usable wavelengths. This problem can be addressed by using absorbance methods, although their relatively smaller detection sensitivity is of concern. This limitation arises because sensitivity of an absorbance detector is in part dependent on the optical path length which in this case is the depth of the microchannel. A brief attempt to calculate the sensitivity of the instrument by incorporating this micrometer sized path length in Beer's Law should clarify where the limitation originates from. A number of techniques can be considered to get around this problem. A bubble cell or a Z- cell and online sample pre-concentration are a few. All the working principle and instrumentation needed for an absorbance detector have been discussed in section 1.7 of chapter one. This work focuses on using a suitable UV set up for detection. The set up as depicted in figure 2.8 includes a UV light source, a micrometer scale adjustable stage, a suitable light aligner mounted on an adjustable stage, a UV-2000 USB detector from (OceanOptics) and two fiber optic cables. The two fiber optic cables from the light source and the detector are connected to the light aligner to align the light path on a straight line. The micrometer scale controllable stage is then adjusted to fit into the light aligner. Finally the microfluidic device is mounted on this stage and detection area is aligned on the light path.

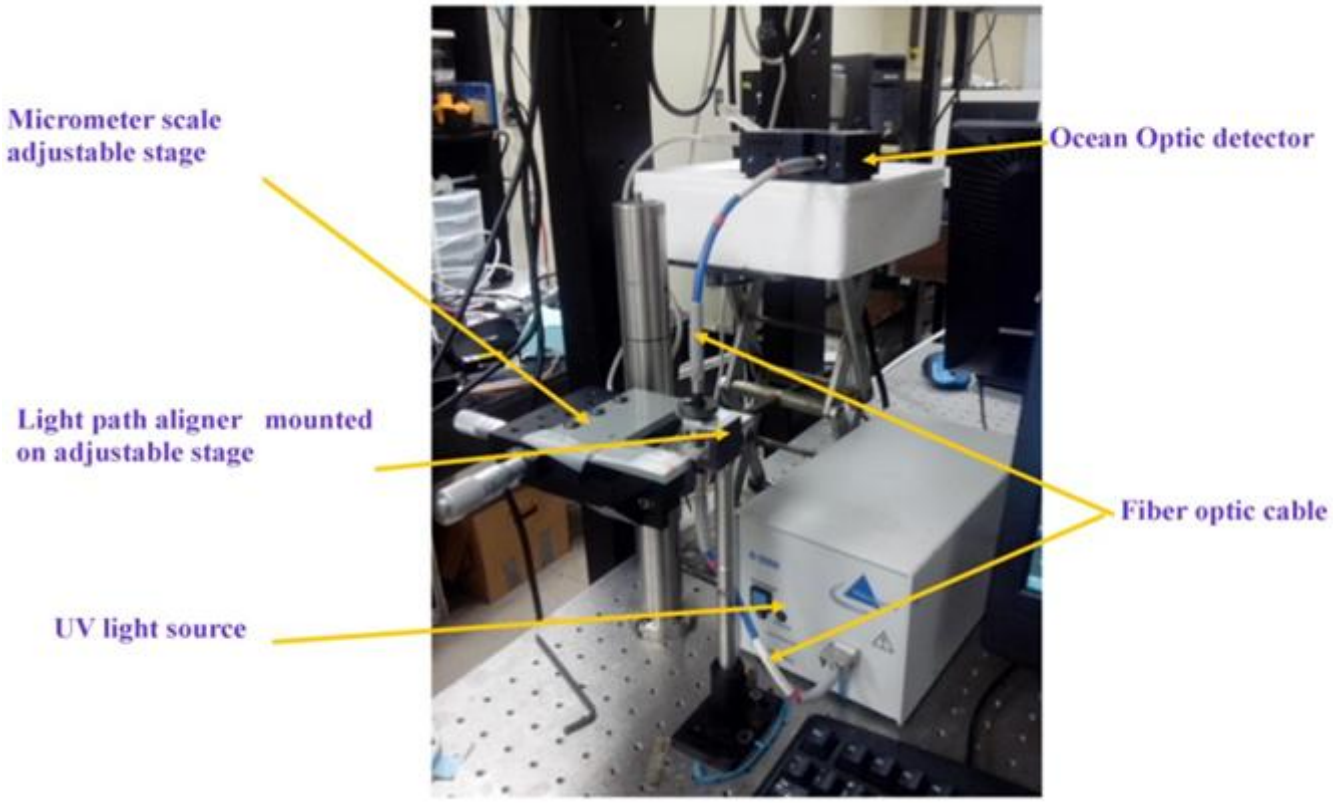

Figure 2.8. UV detector set up.

Summary

This chapter focused on the micro fabrication techniques and operational procedures of microchip capillary electrophoresis. The relative advantages of MCE over conventional CE were discussed to address the motive of conducting MCE experiments. Moreover a suitable detector set up for microfluidic devices is introduced and illustrated. The following chapter will focus on the experimental part of this work.

Chapter Three

Experimental

3.1 Chemicals

PDMS (Sylgard 184®) was obtained from Dow Corning (Midland, MI). Benzophenone and sodium sulfate was purchased from Fisher Scientific (Pittsburgh, PA). Sodium dodecylsulfate (SDS) was obtained from Sigma Chemicals Co. (St. Louis, Mo). 2',7'-dichlorofluorescein (DCF) was obtained from Acros Organics (Morris Palaids, NJ). SU-8 2010 and SU-8 2010 developer were purchased from MicroChem Corp. (Newton, MA). Distilled/deionized water was generated using an E-pure system (Barnstead, Dubuque, IA) and used to prepare all the solutions necessary for the experiments reported. All of the solutions were filtered though 0.45mm PVDF filters purchased from Fischer Scientific before use. 3" by 1" Fused Silica microscope slides obtained from Technical Glass Products (Painesville, OH) were cleaned using Piranha (70% H2S04 +30% H2O2) before use.

Gliadin wheat protein was extracted from 100g of wheat flour using 10ml of 50% propanol in water solution. The extract was centrifuged for 2 min at 1600rpm and the supernatant was collected and stored in eppendorf tube. The flour was a gift from George Lookhart from the United States Department of Agriculture Grain Production Research Center.

3.2 Instrumentation

3.2.1 Mask

Photomasks with the fluidic network pattern necessary for the microfabrication of photo-PDMS devices were designed using AutoCAD 2006 LT (Thompson learning, Albany, NY) software. Figure 3.1 below depicts the fluidic network pattern. The mask contains intersecting fluidic network patterns; the length of each pattern from one access hole to the other is 8cm. The width of the channels is 50µm, except on the curves where the channels narrow to 25 µm. The rationale for this narrowing is to reduce diffusion at the curved areas. The two patterns below the intersection make up the separation/analysis and the waste channels of the device. The design was plotted on a transparency sheet in high resolution (40,000 dots per inch) by Fineline Imaging (Colorado Springs, CO).

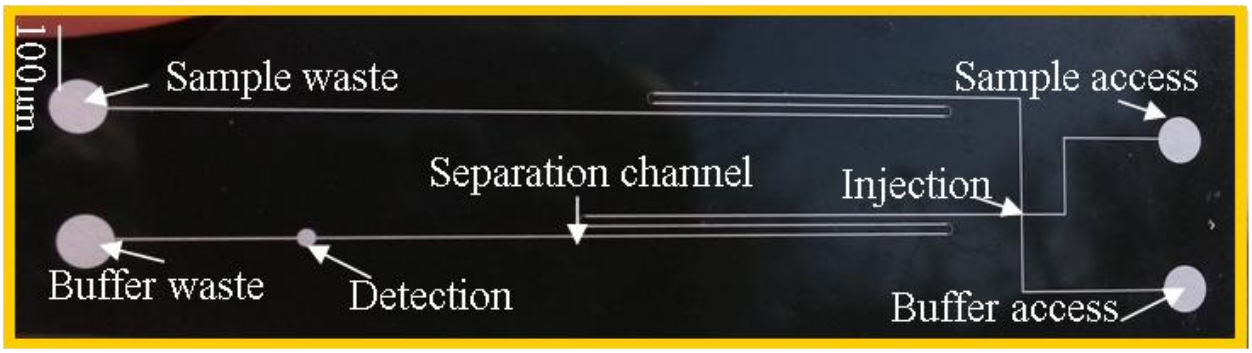

Figure 3.1 Photomask

3.2.2. Device Fabrication

3.2.2.1 Quartz/PDMS device fabrication

A clean 4" by 4" silicon wafer (Silicon Inc., Boise, ID) was used as the substrate for the fabrication of the mold. After mounting it to the spin coater, a 4mL aliquot of SU-8 2010 was deposited on the substrate. The spin coater was programmed at 1500rpm for 40 s to generate a 20µm thick film on the surface. After spin coating, the SU-8 resist was subjected to soft baking. The soft baking protocol includes baking PDMS at 65^0C for 2 min and at 95^0C for 4 min on a hot plate. After soft baking, the photomask was aligned on the top of the SU-8 photoresist and placed in the UV flood exposure cabinet (Oriel Instruments). A 180 mJ/cm^2 dose of UV light was dispensed by programming the UV flood exposure system at 30mW/cm^2 for 6 s. Then the SU-8 coated substrate was post baked once more using the same soft baking protocol. Finally after the substrate was cooled down to room temperature, it was developed by submersion in SU-8 developer bath (propylene glycol monomethyl ether acetate) for 1 min, rinsed with isopropyl alcohol and blow dried by gently blowing nitrogen gas over the channels. After characterizing the channel dimensions using Ambios Technology surface profiler (Santa Cruz, CA), the device was ready for micromolding. For this purpose, 13 g of PDMS elastomer was prepared by mixing a 10:1 (w/w) ratio of the base and curing agent and degassing in a vacuum chamber for 10 min. The PDMS elastomer was then poured onto the master mold and baked in an oven (80^0C for 45 min). Later the cross linked PDMS was peeled off the mold and sealed using a 3" by 1" quartz microscope slide. Prior to sealing, access holes were punched into the PDMS chip and the chip was plasma treated for 1 min in order to get a tight permanent seal.

3.2.2.2 Quartz/PhotoPDMS/Quartz Device Fabrication

The chemistry and significance of photoinitiators for making photo-PDMS as well as the process of fabricating a photoPDMS device has already been discussed in section 2.2. One such common photoinitiator is benzophenone. It is a white crystalline solid with very good solubility in organic solvents such as xylene. Benzophenone is sensitive in the 200-400nm range of the light spectrum and does not react in the presence of visible light thus eliminating the need for dark room conditions during the construction of the device.

The photo-PDMS resist was prepared by mixing a 3% (w/w) ratio of Benzophenone in Xylene solution with PDMS elastomer that was prepared as described above. The photo-PDMS was degassed for 15 min prior to spin coating on a clean quartz substrate. The spin coater was programmed at 3000rpm for 40sec to get a 20µm thick photoPDMS resist. After spin coating the photomask was aligned on the top of the photoPDMS with a gap of 60µm as is illustrated in Figure 3.2 below. The rationale was to avoid adhesion of the photomask to the uncured photo-PDMS. The substrate was then exposed to UV light in a flood exposure system at 30mW/cm^2 for 4min to dispense 72 J/cm^2. The unexposed region of the PDMS was cured by baking in an oven at (120^{0}C for approximately 1 min). Finally the photoPDMS was developed by immersion in a toluene solvent bath for 10-15 s. The fluidic network was sealed by plasma bonding with another quartz substrate that contained drilled access holes.

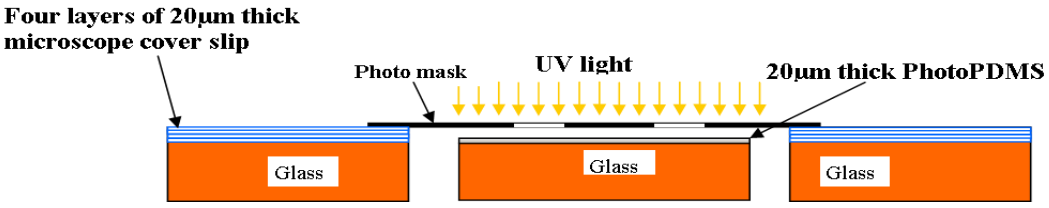

Figure 3.2, Instrumentation for UV exposure of photo-PDMS

Though the chemistry of benzophenone sensitized photo-PDMS is well established, there are several limitations in the fabrication process that need to be addressed. Two such limitations are the long UV exposure time and the extreme sensitivity of feature dimension to the curing step.[44] To investigate these limitations, the exposure time and the curing time were varied from 3-6min and 30-90s respectively. The fluidic channels were investigated visually under an inverted dark field microscope and the dimensions were measure using a stylus surface profiler (Ambios technology; Santa Cruz, CA).

3.3 Sample Injections on Microfluidic Devices

The principle of gated injection is discussed in section 2.3. The injection and run/analysis modes of the boundary gate between two laminar flows can be controlled by manipulating the electric field strength. The electric field strength can be controlled by altering the applied potential at the buffer and the sample reservoir; the two waste reservoirs are connected to the ground. After fabrication of the devices as mentioned above, the chips were prepared for separation experiments by priming them with methanol, then water and finally filling them with 10mM sodium borate buffer that contains 25mM SDS. Four electrodes from the power supply system were dipped into the buffer reservoir (BR), sample reservoir (SR), buffer waste reservoir (BW) and Sample waste reservoir (SW) respectively (Figure 3.3). The power supply system is a suitable in-house built power supply which is controlled with LabView (National Instruments; Austin TX). The LabView software was programmed in such a way to inject a one second sample plug into the separation channel (Table 1 below). (LIF) detection was used to visually investigate the quality of injections by aligning the injection area into to the light path of the

detection system. The response of the fluid flow to the alterations in electric field was recorded as a movie file.

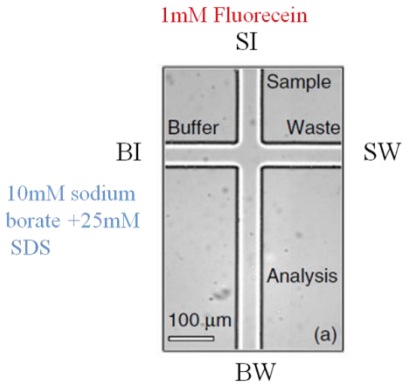

Figure 3.3 Injection techniques in a microchip capillary electrophoresis.

Table 1 Lab view program for performing injection on a micorluidic device.

	Sample introduction (SI)	Buffer introduction (BI)	Sample waste (SW)	Buffer waste (SW)
Run (30s)	1KV	1KV	0KV	0KV
Injection (1s)	1.5KV	0.9KV	0KV	0KV
Run/Analysis (300s)	1KV	1KV	0KV	0KV

3.4 Electrophoretic Separations

After investigating the sample injection performance of the chip, a sample of three amino acids labeled with 250mM fluorescein was injected into the separation channel as described in the above section. After injection of the sample plug the mode of the gate was switched back to the run/analysis mode and programmed to run for 300s. The separated amino acids were detected using (LIF) method. The LIF setup includes a broadband mercury (450-490nm) light source, Nikon bandpass excitation and emission filters and a high resolution Sony CCD color video

camera (Nikon TE2000U, Roper Scientific), both incorporated in an inverted compound microscope. The data was saved as a movie file.

3.5 Characterization of UV Detection System.

The suitable UV detection system setup for microfluidic devices was introduced and discussed in section 2.5 of chapter 2. The setup is similar to the LIF detection setup discussed in section 3.4 above. But in this case the light source and CCD detector were mounted on a suitable light path aligner. After investigating the quality of the injection and separation of the device as mentioned above, the chip was mounted to the adjustable stage of the UV detector set up and aligned into the light path of the detection system. The experiments listed below were conducted to investigate the response of the detector to different sample injections.

3.5.1 Procedure for Detection Limit Determination

10µM, 100µM and 1mM of fluorescein in 10mM sodium borate and 25mM SDS buffer were injected into separation area to investigate the sensitivity of the detector. As described above the power supply was programmed to give a 1 second sample plug length. Three injections of each sample were introduced into the separation channel and run for 300 seconds. The response of the Ocean Optic spectrophotometer (OceanOptics, Dunedin, FL.) throughout the run time was recorded as an absorbance signal in SpectraSuite, a read out software for ocean optics spectrophotometer. Later this data was exported into IgorPro and plotted as absorbance versus time graph.

3.5.2 Procedure or Sample Separation

The single point separation experiment discussed above was conducted using the same setup as the sensitivity in order to investigate the reproducibility of visual investigation by the UV

detector set up. The data was collected and processed in the same manner as for the sensitivity investigations above.

3.6 Wheat Protein Detection Experiment

The gliadin portion of wheat protein was extracted as described in section one of this chapter. After the extraction process one second sample plug was injected into the separation channel and run for 300s. The response of the detector though out the run time is recorded in to Spectrasuite (OceanOptic as previously described. Later these data were exported into IgorPro and plotted as an absorbance versus time graph.

Summary

This chapter focused on the experimental section of this work. Investigations on the fabrication process of the device, quality of injection and separation as well as on the response of the UV detector system were presented in section 2, 3, 4 and 5 respectively. All the relevant data from the experiments discussed in this chapter are presented and elaborated in the following chapter.

Chapter Four

Results and Discussion

4.1 Fabrication

The photochemistry behind and fabrication steps of making a quartz/photoPDMS/quartz devices are was described in chapters two and three. Photo-PDMS was prepared by photosensitizing PDMS using benzophenone, a reactive photoinitiator. Figure 4.1 below depicts a magnified image of a microchannels fabricated by direct writing using UV flood exposure on photo-PDMS resist. The images were taken at 100X magnification using a 10X objective and 10X transfer lens. All these steps were accomplished under ambient light without the need for dark room.

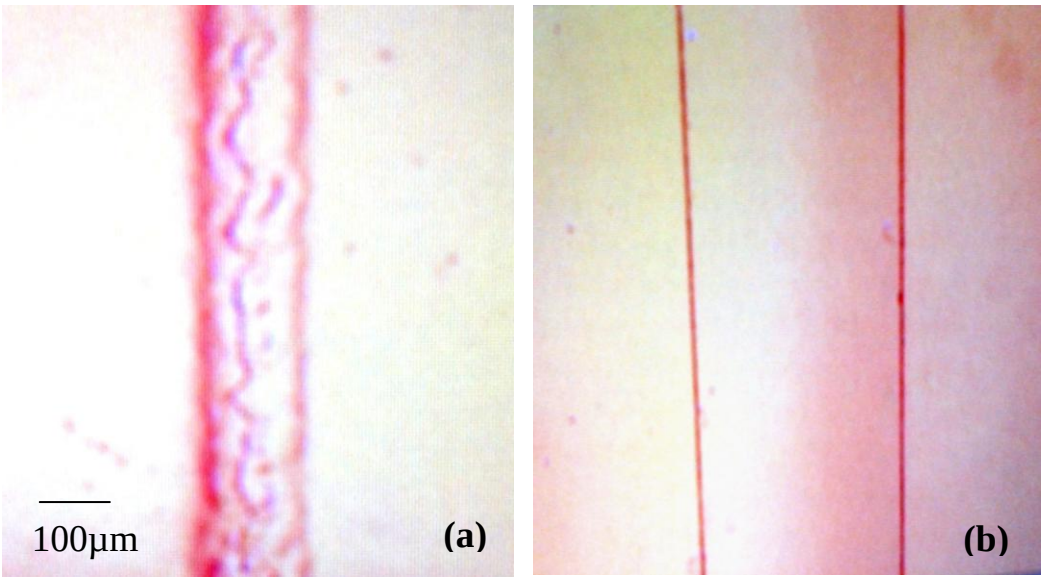

Figure 4.1. (a) residue on the bottom of a 100µm channel, (b) well defined 300 µm channel.

To investigate the effect of exposure time on feature dimension, the UV exposure time was varied from 2-6min. At exposure times below 4min the pattern on the photoPDMS was poorly defined, these may be due to the insufficient time for activating all the benzophenone molecules. On the other hand, although longer exposure time (6min) resulted in better resolved side walls, it leads to widening of the channel by 1.5 times the original pattern on the photomask. Exposure times of 4-5min which resulted in a 20-40% widening of the microchannel were found to be the optimum exposure times.

Another crucial step that determines the feature resolution is the post exposure curing time. During the curing step the unexposed regions of the photo-PDMS are cross-linked to solidify the photo-PDMS resist. The curing temperature and the time play a crucial role in defining feature dimensions. Curing photo-PDMS at lower temperature such as 80^0C oven requires longer baking time (10min) as compared to relatively higher temperature (120^0C for approximately 1min). It was found outdetermined that shorter baking times at higher temperatures leads to optimal feature definition. This could be due to the reflow of photo-PDMS and random diffusion of the reactive photo-initiator radicals [46]. Moreover, baking at 120 ^{o}C for less than 40s resulted in peeling of photo-PDMS during the development step due to under baking. On the other hand baking for more than 70s resulted in formation of photo-PDMS residues at the bottom of the microchannel. This may be partially explained by the reflow property of photo-PDMS and the differences in thermal conductivities of the quartz (1.4W/ m^0C) and photo-PDMS (approximately 0.17W/m^0C). Longer baking time leads to increased reflow at the bottom of the channel whereas the thermal effect is more pronounced than the surface of the photo-PDMS.

4.2 Injection

The results from visual investigation of the injection performance are depicted in figure 4.2 below. These results are in agreement with the injection principles presented in chapter two and three. The boundary gate in figure 4.1a was established by applying 1kV at the sample reservoir (SR) and the buffer reservoir (BR). During injection the potential applied was changed to 1.5kV at the SR and 0.9kV at the BR. This introduced a sample plug in to the separation channel as can be seen in figures 4.2 b and c. Moreover, it was observed that the linear velocity and flow rate increased with increase in applied electric field strength and hence a proportional relationship.

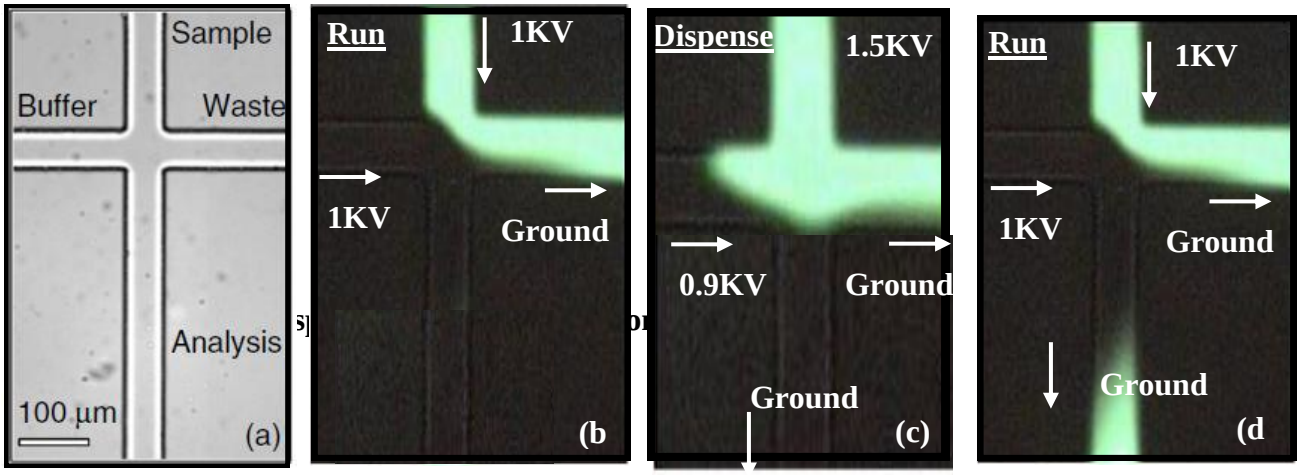

Figure 4.2. Visual inspection of device injection performances.

4.3 Separation

After verifying the injection performance of the device, a sample plug of equimolar mixtures of three amino acids (arginine, tryptophan, and glutamic acid) labeled with fluorescein was injected into the separation channel. The sample mixture was injected by switching the applied voltage to the run/analysis mode by altering the voltages at SR and BR to 1kV and 1.2 kV, respectively. Figure 4.3 below is shows the separation of the mixture into its components.

Figure 4.3. Separation of a mixture of three aminoacids.

4.4 UV Detection

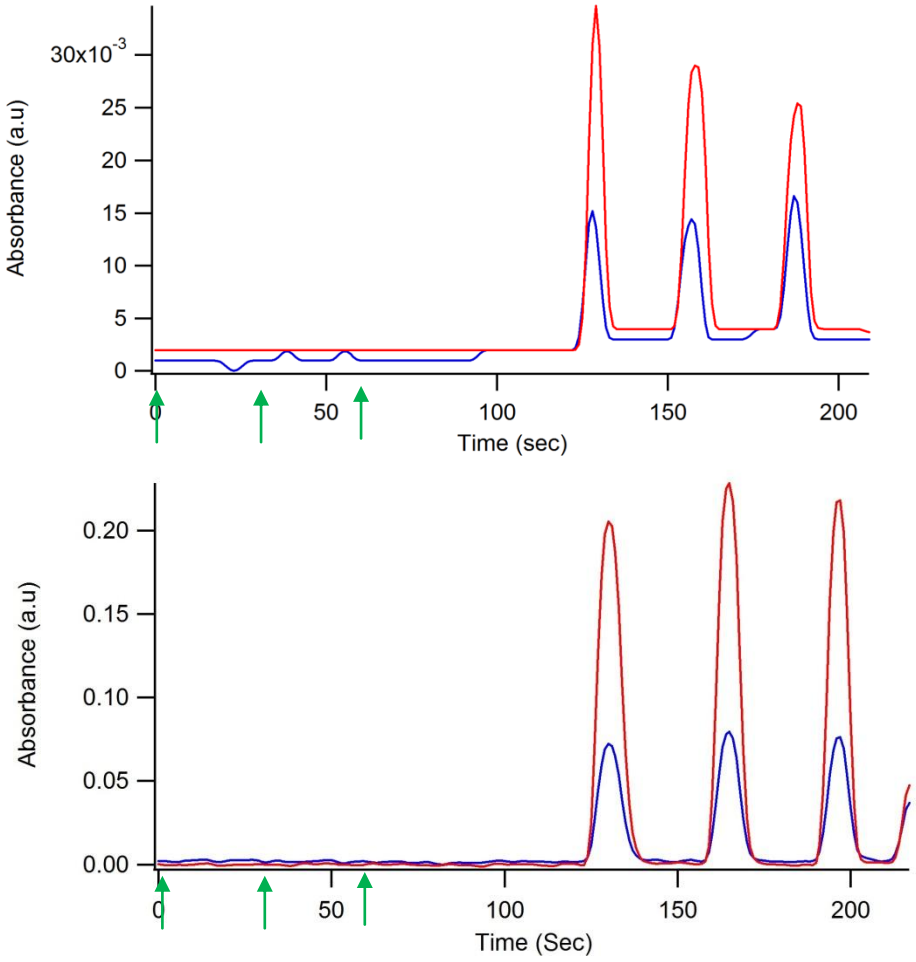

Figure 4.4. Response of a UV detector to (a) three one injections of 100µM FITC (b) three injections of 1mM fluorescein.

After successfully demonstrating the injection and separation performance of the device using LIF detection, the device was aligned with the light path of a suitable lab designed UV detection system as described in previous chapter. A 200µm slit was aligned at the detection area of the device in order to reduce the effect of stray light. Figure 4.4 illustrate the sensitivity detection capability of the of UV detection system. The three peaks in each figure are obtained from a 1s sample injection. The more or less one order of magnitude difference in the absorbance intensities is in complete agreement with the one order of magnitude difference in sample concentrations (Table 2 below). Moreover, peak positions of all the six injections as well as the absorbance peak intensities from the three injections of a sample illustrate the ability of the UV detector system to generate reproducible results.

Table 2. Migration time vs absorbance at 500nm of three injections of a 100µM and 1mM fluorescein injections.

Concentration	Injection	Migrationtime (500nm)	Absorbance (a.u)
100µM	1 (0s)	124s	$3.2x10^{-2}$
	2 (30s)	157s	$2.8x10^{-2}$
	3 (60s)	185s	$2.7x10^{-2}$
1mM	1 (0s)	131s	$2.2x10^{-1}$
	2 (30s)	164s	$2.7x10^{-1}$
	3 (60s)	198s	$2.5x10^{-1}$

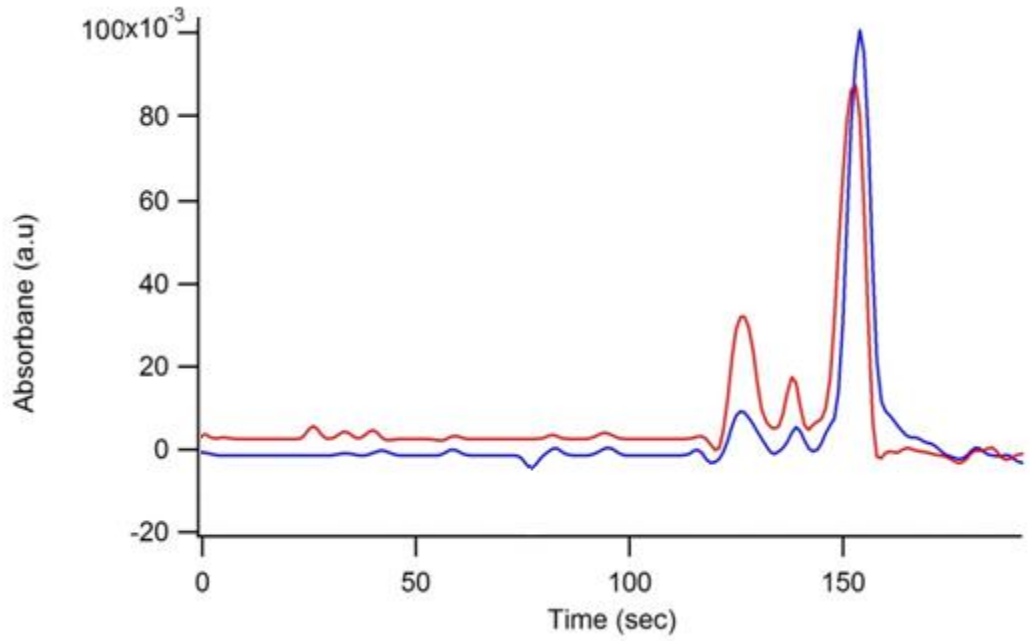

Figure 4.5. Separation of a mixture of three amino acids into its three components.

The three peaks were detected 5.5cm away from the junction where a one second sample plug was introduced into the separation channel. As can be seen from the figure, the three amino acids reach the detection point at three different migration times. Table 1 below lists the migration times of the three amino acids as well as the resolution between two peaks.

Table 3. Migration time of three amino acid peaks and their resolution.

Peak	Migration time(s) at 250nm	Width of Peak	Resolution at 250nm	Migration time (s) at 500nm	Width of Peak	Resolution at 500nm
A	125	9		126	11.4	
B	137	5.7	**1.6**	137	7	**1.2**
C	157	11.4	**2.5**	156	11.4	**2.06**

4.5 Wheat protein separation and detection

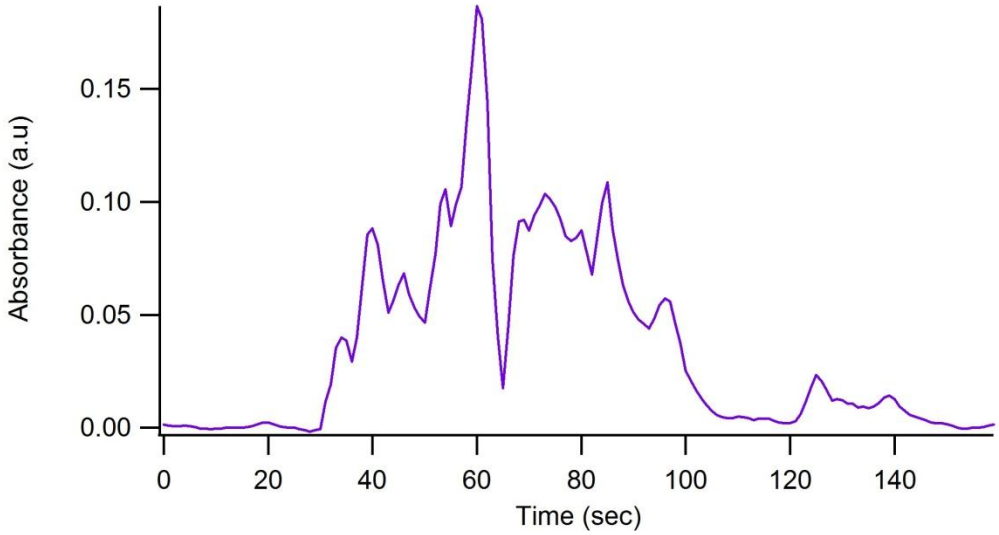

Figure 4.6. Separation and detection of wheat gliadin protein.

Figure 4.6 above depicts the response of the UV detector system to a one second injection of gliadin. After introducing the sample, the separation was achieved by applying 1.4kV though out the run mode. This data was generated by positioning the detector 4.5cm away from the injection area. Although further investigations are needed to optimize the separation conditions this figure successfully demonstrates the applicability of these method to separate and detect gliadin portion of wheat protein.

Summary

This chapter presented the results of the experiments conducted in this work. The limitations of the photo-PDMS fabrication step, the quality of injection and separation of the device as well as the sensitivity of the UV detector system were presented and discussed. Moreover, the applicability of the method for separation and detection of wheat gliadin proteins has been demonstrated.

Conclusion and Future work

This work primarily focused on the use of Capillary Electrophoresis as a separation technique. Furthermore, the application of Capillary Electrophoresis (CE) on microfluidic devices was discussed. Microfabrication techniques of PDMS and photosensitized PDMS (photoPDMS), a UV detector for microfluidic devices and its application for the detection of wheat proteins were the major themes of this work.

In this project, a hybrid quartz/photoPDMS/quartz microfluidic device was successfully fabricated using a rapid prototyping technique without the need of a master template. The effect of UV exposure time and curing time on the feature dimensions of photoPDMS were investigated. Moreover injection and separation performances of the devices were reproduced using a UV detector. Finally the ability of the setup to separate and detect wheat gliadin proteins was successfully demonstrated. Future work will focus on the optimization of the separation and detection performances of the device and the UV detector as well as application to a wide variety of analytical problems.

References

1. Heiger, D. N. *High Performance Capillary Electrophoresis –An Introduction*; 2nd ed.; Hwlett-Packard Company: France, 1992.
2. Jorgenson, J. W., Lukacs, K. D., *Clinical chemistry* **1981**, *27*. 1551-1553.
3. Cieslik, E., Niedospial, A., Mickowska, B., *Zywnosc-Nauka Technologia Jakosc* **2008**, *15*. 5-14.
4. Dong, Y. Y., *Trends in Food Science & Technology* **1999**, *10*. 87-93.
5. Marsh, A., Broderick, M., Altria, K., Power, J., Donegan, S., Clark, B., *Methods in molecular biology* **2008**, *384*. 205-245.
6. Rabel, S. R., Stobaugh, J. F., *Pharmaceutical research* **1993**, *10*. 171-186.
7. Kostal, V., Katzenmeyer, J., Arriaga, E. A., *Analytical Chemistry* **2008**, *80*. 4533-4550.
8. Fukushi, K., Takeda, S., Chayama, K., Wakida, S., *Journal of Chromatography A* **1999**, *834*. 349-362.
9. Fung, Y. S., Tung, H. S., *Electrophoresis* **1999**, *20*. 1832-1841.
10. Jorgenson, J. W., Lukacs, K. D., *Science* **1983**, *222*. 266-272.
11. Jorgenson, J. W., *Science* **1984**, *226*. 254-261.
12. Terabe, S., Otsuka, K., Ichikawa, K., Tsuchiya, A., Ando, T., *Analytical Chemistry* **1984**, *56*. 111-113.
13. Terabe, S., Otsuka, K., Ando, T., *Analytical Chemistry* **1985**, *57*. 834-841.
14. Paulus, A., Ohms, J. I., *Journal of chromatography* **1990**, *507*. 113-123.
15. Cohen, A. S., Najarian, D. R., Karger, B. L., *Journal of chromatography* **1990**, *516*. 49-60.
16. Wehr, T., Zhu, M., Rodriguez, R., Burke, D., Duncan, K., *American biotechnology laboratory* **1990**, *8*. 22-29.
17. Gebauer, P., Bocek, P., *Electrophoresis* **1997**, *18*. 2154-2161.
18. Helmholtz, H.Z. About electrical interfaces (translated title), Annal. Phys. Chem., 1879, 7, 337.
19. Smoluchowski, M. V. (1905) Elektrosche kataphorese. Physik. Z. 6, 529.
20. Skoog, D.A.; Holler, F.; Crouch, S.R. Principles of Instrumental analysis, **2007**.
21. Morteza, G.Khaledi. High Performance Capillary Electrophoresis, Theory, Techniques and Applications, **1998**.)

22. M. Albin, P.D. Grossman, and S.E. Moring, *Anal.Chem* **65**, 489A-497A (1993).
23. W. Beck, R. banHoek, and H. Engelhardt, *Electrophoresis* **14**, 540-546 (1993)
24. T. Wang, U.H. Aiken, C.W. Huie, and R. A. Hartwick, *Anal.Chem* **63,** 1372-1376
25. Miniaturization of Analytical Systems: Principles, Designs and Applications Angel Rios, Alberto Escarpa and Bartolome Simonet © 2009 John WIley & Sons.
26. J. C. McDonald and G. M. Whitesides, "Poly(dimethylsiloxane) as a material for fabricating microfluidic devices," Acc. Chem. Res., **35**, (2002), 491–499.
27. Manz, A., Harrison, D. J., Verpoorte, E. M. J., Fettinger, J. C., Paulus, A., Ludi, H., Widmer, H. M., J. Chromatogr. 1992, 593, 253-258.
28. Greenway, G. M., Haswell, S. J., Petsul, P. H., Anal. Chim. Acta **1999**, 387, 1-10.
29. Vrouwe, E. X., Luttge, R., Olthuis, W., van den Berg, A.,J. Chromatogr. A **2006**, 1102, 287-293.
30. Vrouwe, E. X., Luttge, R., van den Berg, A., Electrophoresis **2004**, 25, 1660-1667.
31. Vrouwe, E. X., Luttge, R., Olthuis, W., van den Berg, A.,Electrophoresis **2005**, 26, 3032-3042.
32. Sirichai, S., de Mello, A. J., Analyst **1999**, 125, 133-137.
33. Garcia, C. D., Engling, G., Herckes, P., Collett, J. L., Henry, C. S., Environ. Sci. Technol. 2005, 39, 618-623.
34. Reyes, D. R.; Iossifidis, D.; Auroux, P. A.; Manz, A. Micro Total Analysis Systems. 1. Introduction, Theory, and Technology. Anal. Chem. **2002**, 74, 2623–2636.
35. Mu, X.; Liang, Q. L.; Hu, P.; Ren, K. N.; Wang, Y. M.; Luo, G. A. Laminar Flow Used as "Liquid Etch Mask" in Wet Chemical Etching to Generate Glass Microstructures with an Improved Aspect Ratio. Lab Chip 2009, 9, 1994–1996.
36. Jacobson, S. C., Moore, A. W., & Ramsey, J. M. **(1995**). Fused quartz substrates for microchip electrophoresis. *Analytical Chemistry*, *67*(13), 2059-2063. doi:10.1021/ac00109a026
37. Becker, H. and Locascio, L. (2002) Polymer microfluidic devices. *Talanta* **56,**267–287.
38. Shadpour , H. , Musyimi , H. , Chen , J. F. and Soper , S. A. (**2006**) Physiochemical properties of various polymer substrates and their effects on microchip electrophoresis performance. J. Chromatogr. A 1111 , 238 – 251
39. Hayashi, T. *Comprehensive Asymmetric Catalysis*, Springer.

40. Mukhopadhyay, R. When PDMS Isn't the Best. Anal. Chem. **2007**, 79, 3248–3253.
41. C.-M. Cheng, B. Li, P.R. LeDuc, Appl. Phys. Lett. 87, 164104 (2005)
42. S.P. Desai, B. Taff, J. Voldman, Langmuir **24**, 575 (2008)
43. A. Chayet, C.A. Sandstedt, S.H. Change, P. Rhee, B. Tsuchiyama, D. Schwartz, Am. J. Ophthalmol. 147, 393 **(2009**)
44. Choi KM, Rogers JA (2003) A photocurable poly(dimethylsiloxane) chemistry designed for soft lithographic molding and printing in the nanometer regime. J Am Chem Soc **125**:4060–4061
45. McDonald , J. C. , Duffy , D. C. , Anderson , J.R. , Chiu , D. T. , Wu , H. K. , Schueller , O. J.A. , Whitesides , G. M. (2000) Fabrication ofmicrofluidic systems in poly(dimethylsiloxane) .*Electrophoresis* **21** , 27 – 40 .
46. Preetha Jothimuthu *et al* 2009 *J. Micromech. Microeng.* **19** 045024